Title

Nanogold based protein localization enables subcellular visualization of cell junction protein by SBF-SEM.

Authors

Liang, Feng-Xia
Sall, Joseph
van Opbergen, Chantal
et al.

Publication Date

2023

DOI

10.1016/bs.mcb.2022.12.020

Peer reviewed

HHS Public Access

Author manuscript

Methods Cell Biol. Author manuscript; available in PMC 2023 October 28.

Published in final edited form as:

Methods Cell Biol. 2023 ; 177: 55–81. doi:10.1016/bs.mcb.2022.12.020.

Nanogold based protein localization enables subcellular visualization of cell junction protein by SBF-SEM

Feng-Xia Liang[a,b,*], **Joseph Sall**[a], **Chris Petzold**[a], **Chantal J.M. van Opbergen**[c], **Xiangxi Liang**[a], **Mario Delmar**[c]

[a]Microscopy Laboratory, Division of Advanced Research Technologies, New York University Grossman School of Medicine, New York, NY, United States

[b]Department of Cell Biology, New York University Grossman School of Medicine, New York, NY, United States

[c]Leon H Charney Division of Cardiology, Department of Medicine, New York University Grossman School of Medicine, New York, NY, United States

Abstract

Recent advances in volume electron microscopy (vEM) allow unprecedented visualization of the electron-dense structures of cells, tissues and model organisms at nanometric resolution in three dimensions (3D). Light-based microscopy has been widely used for specific localization of proteins; however, it is restricted by the diffraction limit of light, and lacks the ability to identify underlying structures. Here, we describe a protocol for ultrastructural detection, in three dimensions, of a protein (Connexin 43) expressed in the intercalated disc region of adult murine heart. Our protocol does not rest on the expression of genetically encoded proteins and it overcomes hurdles related to pre-embedding and immunolabeling, such as the penetration of the label and the preservation of the tissue. The pre-embedding volumetric immuno-electron microscopy (pre-embedding vIEM) protocol presented here combines several practical strategies to balance sample fixation with antigen and ultrastructural preservation, and penetration of labeling with blocking of non-specific antigen binding sites. The small 1.4 nm gold along with surrounded silver used as a detection marker buried in the sample also serves as a functional conductive resin that significantly reduces the charging of samples. Our protocol also presents strategies for facilitating the successful cutting of the samples during serial block-face scanning electron microscopy (SBF-SEM) imaging. Our results suggest that the small gold-based pre-embedding vIEM is an ideal labeling method for molecular localization throughout the depth of the sample at subcellular compartments and membrane microdomains.

[*]*Corresponding author:* fengxia.liang@nyulangone.org.

Author contribution

FL, CvO, and MD conceived the study. FL, JS and CP drafted the manuscript. JS, CP, CvO and XL performed the experiments, imaging, and image processing. CvO performed data analysis. MD and CvO critically revised the manuscript. All authors approved the final version.

1 Introduction

Since the 1960s, after the implementation of glutaraldehyde-osmium tetroxide as standard fixative for biological samples (Sabatini, Bensch, & Barrnett, 1963), electron microscopy (EM) has been a powerful tool for biologists, leading to many discoveries of cell organelle structures. A major limitation inherent to standard EM is the fact that visualization is only resolved in one plane. Recent advances in volume electron microscopy (vEM) have overcome this major hurdle, now allowing for the study of tissues, cells and model organisms in three-dimensions at nanometric resolution (Peddie et al., 2022). Beside morphological characterization, subcellular protein localization is one of the key steps to understand the function of macro-molecules. Given the fact that diffraction-limited light microscopy does not provide sufficient spatial resolution, when combining molecular detection methods, immunelabeling electron microscopy (Immuno-EM, or IEM) is the only technique to localize, with nanometric resolution, a protein within its native structural landscape (Koster & Klumperman, 2003).

Pre-embedding immunolabeling electron microscopy techniques (preembedding IEM, immunolabeling before the specimens are embedded in resin) have provided superior opportunities for volumetric localization of macromolecules, and for the identification of unexpected biological events. The use of immunolabeling on vEM is challenging due to two main reasons: penetration of the labeling, and preservation of tissue. With frozen sections of agar-embedded cell pellets, one can achieve partial penetration of a biomarker on the cells that were sectioned (Melo, Morgan, Monahan-Earley, Dvorak, & Weller, 2014), but they cannot achieve the labeling of multi-cell layers in large tissue sample volumes. Also, freeze damage might affect the integrity of cell membranes in an uncontrolled manner. Genetic encoded analogues of GFP molecules such as miniSOG (Perkins, 2014; Shu et al., 2011), APEX and APEX2 (Lam et al., 2015; Martell et al., 2012) have been successful at providing electron dense signals upon exposure to diaminobenzidine tetrahydrochloride (DAB) in cells or tissues, which eliminates concerns regarding antibody penetration. Yet, the tag in the gene construct might affect the behavior of some molecules, and diffuse DAB precipitation signals are not appropriate for proteins that localize to the cell junctions, since it is hard to differentiate the structures within the two opposing membranes.

Colloidal gold particles have been widely used as probes for subcellular protein localization of two-dimensional post-embedding on section immunolabeling (Faulk & Taylor, 1971; Kerr et al., 1998; Liang et al., 2005; Roth, Bendayan, & Orci, 1978). Given their limited penetration, colloidal golds are not able to label the entire cell, even after cell membrane permeabilization (Hainfeld & Furuya, 1992). Physical manipulation has been applied by perforating a single tunnel through the cell using UV laser perforation (Jimenez & Post, 2012) in order to help the colloidal gold enter in vitro cultured cells, however, intracellular diffusion of large gold particles (at least 5nm in diameter in order to be visualized under EM with embedded sample) is limited by the highly crosslinked cytoplasm of the cell after fixation (Baschong & Stierhof, 1998; Hagiwara, Aoki, Suzuki, & Takata, 2010); in addition, a portion of cell structure is damaged by the laser, making it impossible to achieve whole cell 3D reconstruction.

To increase penetration of the probe and achieve volumetric immunolabelling, we utilized small gold called nanogold (NG, 1.4 nm in diameter) which is conjugated covalently to Fab' fragment (one-third the size of a whole IgG (Melo et al., 2014)). Nanogold is a neutral molecule that is stable in a wide range of pH's and ionic charges, it can also be covalently linked to a fluorophore to form FluoroNanogold (FNG) for visualization of a given antigen using correlative light and electron microscopy (CLEM) or multimodal microscopy (Cheutin et al., 2007; Giepmans, 2008). Overall, these very small probes have greatly improved our ability to penetrate inside cells or tissue, providing excellent visualization of cellular compartments and membrane microdomains.

Gap junctions are intercellular channel-forming structures that allow for the passage of ions and small molecules between cells. In the heart, they are critical for the synchronous beating of the cardiac myocytes (Fig. 1A). The most abundant gap junction protein in the heart is Connexin 43 (Cx43, Fig. 1B). Cx43 oligomerizes as a hexamer that, in each cell, forms a hemichannel. Docking of two hemichannels in the intercellular space forms a full gap junction. Previous studies have shown that functional Cx43 "orphan" hemichannels are abundant in cardiac myocytes consequent to the loss of plakophilin – 2 (PKP2), a desmosomal protein (Kim et al., 2019). Loss or mutations in PKP2 are known to be responsible for most cases of gene-positive arrhythmogenic right ventricular cardiomyopathy (ARVC) (Gerull et al., 2004; Grossmann et al., 2004). We applied NG and FNG labeling of Cx43 using pre-embedding IEM on cardiac vibratome sections after permeabilization by a detergent, to visualize in three dimensions gold labeled-Cx43 in gap junction plaques of adult murine heart. Serial block-face scanning electron microscopy (SBF-SEM) imaging of PKP2-deficient adult murine hearts revealed the separation of the intercellular membranes, including the areas populated by Cx43, consequent to desmosomal deficiency, and the presence of long strings of Cx43-labelled proteins in only one of the cell membranes, consistent with the notion of orphan Cx43 hemiplaques (van Opbergen et al., 2022).

2 Before you begin

Timing: 1–2h

1. ddH_2O: Millipore deionized water
2. PBS: 0.1M phosphate buffer saline, pH 7.2–7.4, autoclaved
3. PB: 0.1M phosphate buffer, pH 7.2–7.4
4. Fixative solution
   a. 4% PFA fixative solution: 4% paraformaldehyde (PFA, v/v) in PBS, pH 7.2–7.4
   b. 4% PFA and 0.5% GA fixation solution: 4% paraformaldehyde (PFA, v/v), 0.5% glutaraldehyde (GA, v/v) in PBS, pH 7.2–7.4
   c. 2.5% GA fixative solution: 2.5% GA (v/v) in PB, pH 7.2–7.4

d. 0.5% OsO_4 solution: 0.5% osmium tetroxide (OsO_4, v/v) in PB, pH 7.2–7.4

5. 50mM glycine: 37.5mg glycine dissolved in 10mL PBS
6. Permeabilization buffer: 0.05% Triton X-100 (v/v) in PBS
7. Blocking solution: 3% bovine serum albumin (BSA, w/v) in PBS
8. Incubation buffer: 1% BSA (w/v) in PBS
9. 0.02M sodium citrate buffer: 2.58 g sodium citrate ($Na_3C_6H_5O_7$) dissolve in 400mL ddH_2O. Using NaOH to adjust pH to 7.0, then add ddH_2O to make total of 500mL
10. 0.5% UA: 0.5% uranyl acetate (w/v) in ddH_2O, stored in the dark at 4°C
11. Hard Epon and Durcupan (see Table 1)

3 Key resources table

Reagent or resource	Source	Identifier
Antibodies		
Rb × Ms Connexin 43 (Cx43) antibody, C-terminus cytosolic	Millipore Sigma, USA	Cat # AB1728-25UG
Nanogold®—Fab' goat anti-rabbit IgG (H+L) (NG)	Nanoprobes.com, USA	Cat # 2004
Alexa Fluor 546®—FluoroNanogold™ Fab' goat anti-rabbit IgG (H+L) (FNG)	Nanoprobes.com, USA	Cat # 7404
Biological samples		
Heart		
Chemicals		
16% paraformaldehyde	Electron Microscopy Sciences, USA	Cat # 15700
25% glutaraldehyde	Electron Microscopy Sciences, USA	Cat # 16019
4% osmium tetroxide	Electron Microscopy Sciences, USA	Cat # 19150
Glycine	Fisher Scientific, USA	Cat # G46-500
Bovine serum albumin	Sigma-Aldrich, USA	Cat # 9048-46-8
Sodium citrate	Ladd Research, USA	Cat # 20325
Triton X-100	Sigma-Aldrich, USA	Cat # T-9284
HQ silver enhancement kit	Nanoprobes.com, USA	Cat # 2012
Uranyl acetate	Electron Microscopy Sciences, USA	Cat # 23620
200 proof ethanol	Electron Microscopy Sciences, USA	Cat # 15055
Acetone	Electron Microscopy Sciences, USA	Cat # 10012
EMbed-812 embedding kit	Electron Microscopy Sciences, USA	Cat # 14121
Durcupan A, B, C, D	Fluka or Sigma, USA	Cat # 44611-44614
Experimental models: Organisms/strains		
C57BL/6 mouse		
Cardiomyocyte-specific, tamoxifen activated PKP2 knockout mice (PKP2cKO) (14 days post tamoxifen injection)		
Software and algorithms		

Reagent or resource	Source	Identifier
ImageJ	Preibisch, Saalfeld and Tomancak	2009
ORS dragonfly	Object Research Systems Inc.	4.1.0.647
Other		

4 Materials and equipment

- Nutator, BD CLAY ADAMS® brand, model no. 421105, VWR, USA
- Orbital shaker, Troemner™ Talboys™ standard analog 1000 orbital shaker, USA
- Vibratome, Leica VT1200S, Leica Biosystems, USA
- Leica EM UC6 ultramicrotome, Leica Microsystems, USA
- Zeiss Stereo microscope, Stemi508, Carl Zeiss Microscopy, Germany
- Zeiss Axio Observer epifluorescence and crossed-polarization microscope (inverted), Carl Zeiss Microscopy, Germany
- CCU-010 HV coating system, Rave Scientific, USA
- Denton Vacuum DESK V sputter coater, Denton Vacuum, USA
- Talos 120C Transmission Electron Microscope, Thermo Fisher Scientific, USA
- Gemini300 VP Field Emission SEM equipped with Gatan 3View automatic microtome unit and 2nd generation Focus Charge Compensation (FCC), Carl Zeiss Microscopy, Germany
- 24 well tissue culture plate, Corning Incorporated, Cat # 353047, USA
- Camel hair brush, Ted Pella, Inc., Cat # 11860, USA
- Mini rotator, Glas-Col, Cat # 099A MR1512, USA
- ACLAR embedding film, Ted Pella, Inc., Cat # 10501–10m, USA
- Super glue, Loctite products.com, Ireland
- Conductive silver epoxy, Chemtronics CW2400 Epoxy, USA
- Gatan 3View® system SEM pin stub, Electron Microscopy Sciences, Cat #75959–01, USA
- Diatome Diamond Knife, Diatome, Switzerland
- Slot grids, formvar support 2×1mm Cu grids, Cat # FF2010-CU, Electron Microscopy Sciences, USA
- 60°C oven
- 100°C oven

5 Step-by-step method details

The work flow of the pre-embedding immuno—SBF-SEM experimental procedure is demonstrated in Fig. 2, detailed step-by-step method listed below.

5.1 Sample fixation

Timing: ~3h plus ~10h fixation

1. Control and PKP2cKO mice were anesthetized by inhalation of 100% CO_2.
2. Mice were fixed in the supine position with needle/tape and cardiac perfused with PBS first to clean out the blood, then continue perfusion with freshly made 4% PFA.
3. The chest of mouse was opened using a scissor.
4. The heart was dissected, cannulated, rinsed with PBS briefly, then collected in a 15mL falcon tube filled with 10mL freshly made 4% PFA and fixed overnight at 4°C.
5. The heart was removed from fixative solution and placed in a 60mm cell culture dish.
6. The heart was gently dab dried with a piece of Kimwipe paper, and mounted on a vibratome using super glue.
7. Cross sections of 200μm thickness were collected from the heart by vibratome and sections were collected in PBS on ice.
8. Sections were transferred into a 24 well tissue culture plate using a camel hair brush. One section was placed per well, each well contained 1mL of 4% PFA fixative solution (Fig. 3A).

Pause Point: (vibratome sections can be stored in 2% PFA in PBS at 4°C, for up to 2 weeks.)

Note:

1. Fixative solution should be made freshly at the day of use, to allow optimal fixation.
2. Cross sections are used to have the ventricle and atrium of the heart represented in each section.
3. Considering that the penetration of nanogold can reach up to 40μm (Robinson & Vandre, 1997) on both sides of the section, we choose vibratome section of 200 μm thickness. That allows easy handling of the sections during sample processing.
4. Special tissue samples as the cornea are not recommended to be stored in aldehyde, due to its unique lipid composition on the cell membrane (unpublished data).

Critical: Sample fixation is crucial for protein localization at the ultrastructural level, since it is challenging to maintain a good balance between tissue antigenicity and morphology. Freshly made paraformaldehyde can quickly penetrate into the cells or tissues and crosslink between proteins, but prolonged washing or storage in buffer after fixation should be avoided, since it would result in fixation reversal (Newman & Hobot, 1993). Glutaraldehyde has been widely used as fixative as its stronger crosslinking qualities result in better morphological preservation of the tissue. However, using a concentration of glutaraldehyde above 1% would likely destroy the antigenicity of important proteins. Given its strong auto-fluorescence (Seveus, Vaisala, Kojola, Roomans, & Soini, 1994), higher concentrations of glutaraldehyde fixation are not recommended for correlative microscopy, and the most optimal would be the use of a concentration between 0.1% and 0.5% (Newman & Hobot, 1993). For fixing animal tissues, 2–4% paraformaldehyde is recommended for the perfusion fixation, followed with a mixture of 2–4% paraformaldehyde plus 0.1–0.5% glutaraldehyde for post fixation after tissue dissection. The concentration of glutaraldehyde to be used in the post fixative solution depends on the sensitivity of each unique antigen, this can be tested using fluorescent microscopy. For example, try to fix the cells or tissues with 0.1%, 0.2%, 0.5% and 1% glutaraldehyde in 2% or 4% paraformaldehyde/PBS, apply the primary antibody and fluorophore conjugated secondary antibody, and check the fluorescent signal under fluorescent microscope. If a positive signal can be achieved in 0.1%, 0.2%, and 0.5% but not in 1% glutaraldehyde fixed sample, then choose 0.5% glutaraldehyde for the EM experiment. The higher percentage of glutaraldehyde, the better morphological tissue preservation will be achieved. Perfusion fixation is highly recommended for observation of mitochondria and muscle fiber structures, due to the contracting nature of muscle tissue (Liang et al., 2021). Previous studies from our lab have shown that chemical fixation or high pressure freezing - freeze substitution after perfusion fixation produces a similar ultrastructural preservation of murine cardiac intercalated disc (ID) structures (Cerrone et al., 2012; Delmar & Liang, 2012; Leo-Macias et al., 2016a, 2016b; Leo-Macias,Liang,& Delmar,2015).In this experiment, we confirmed that perfusion coupled with chemical fixation caused no morphological alterations of the mouse ID.

5.2 Immunolabeling

Timing: ~10h plus ~20h antibody incubation

1. Sections are post-fixed with 4% PFA and 0.5% GA fixation solution for 1h at room temperature (RT) before immunolabeling.
2. Wash with PBS, 3×10min, @RT
3. Incubate with 50mM glycine to quench unbound aldehydes, 30min, @RT
4. Wash with PBS, 15min, @RT
5. Permeabilization with 0.05% Triton X-100, 30min, @RT
6. Blocking with 3% BSA/PBS, 60min, @RT.
7. Primary antibody incubation in 1% BSA/PBS (anti-Cx43 rabbit polyclonal antibody,1:50 dilution), 2h @RT, then overnight @4°C (for a negative control, incubate sample in incubation buffer without primary antibody).

8. Wash with incubation buffer, 6×30min, @RT
9. Secondary antibody incubation in 1% BSA/PBS (Nanogold Fab' or FluoroNanogold Fab' anti-rabbit conjugated, 1:200 dilution), 2h @RT, then overnight @4°C
10. Wash with incubation buffer, 4×30min, @RT
11. Wash with PBS, 2×30min, @RT
12. The sections underwent another fixation step with 2.5% GA, 2h @RT

Pause Point: (sample can be stored overnight @ 4°C after GA fixation).

5.3 Optional steps

Timing: ~1h—After step 11 before GA fixation, imaging can be performed using an inverted epifluorescence microscope, in case FNG was applied as secondary antibody for correlative microscopy (van Opbergen et al., 2022). Both fluorescence and DIC/phase imaging are required in low and high magnification in order to correlate the position and shape of the target during the EM sample trimming stage.

Note:

1. All steps were performed on an Orbital shaker at low speed (set as 2).
2. Permeabilization reagent and concentration of the detergent should be titrated accordingly to balance the cell permeability and preservation of the ultrastructure.
3. Blocking buffer and antibody incubation buffer can be varied depending on specificity of each antibody.
4. 200–300μL diluted antibody solution should be sufficient to cover each section on a 24-well dish.
5. For FNG labeled samples, steps 9–11 need to be performed in the dark. The plate can be wrapped in aluminum foil.
6. Seal the dish using parafilm during the antibody incubation step to avoid evaporation of the solution.
7. To increase the binding specificity and penetration of the antibody, it is preferred to incubate the antibody first for 2h at room temperature, before incubating it overnight at 4°C.
8. Large volume washing steps are important for reducing the background of immunolabeling. 1mL solution per well is recommended for all steps beside antibody incubation.
9. Example of light microscopy imaging setting: Zeiss Axio Observer microscope with Plan-Neofluar 10x/0.3NA for tiling imaging at low magnification, Plan Apochromat 20x/0.8NA and Plan-Neofluar 40x/0.9NA lenses for high-resolution imaging.

6 Critical: Antibody specificity is very important for the success of IEM experiment

Any antibody used for IEM, needs to be tested by light microscopy first. Pick only those antibodies with limited background staining and a clear positive signal for EM processing. The same blocking and incubation buffer protocol can be used for preembedding IEM as used for light microscopy staining, even though overall a 10x higher antibody concentration is recommended for post-embedding of IEM labelled sections (Griffiths, 1993). For NG based pre-embedding IEM, the antibody might need to be diluted even 2–3x more than in the case of light microscopy, due to amplification of silver enhancement. For this matter, a negative control sample is essential for interpretation of the final results. The best negative control would be to apply pre-immune serum of the same animal which was used to generate the antibody, or the sample with abolished antigen. In reality, we recommend to set up a control sample omitting the primary antibody, thereby testing the specificity of the secondary antibody.

6.1 Silver enhancement

Timing: ~3h

1. Wash with ddH_2O thoroughly, 6×10min @RT
2. Wash with 0.02M sodium citrate buffer, 3×5min @RT
3. Transfer each section to a fresh well at last wash for silver enhancement
4. Perform silver enhancement under safety red light in the dark room using equal amounts of three components, 8min @RT:
    a. Mix equal amount of solution A (initiator) and B (moderator)
    b. Add same amount of C (activator) and mix thoroughly
    c. Add enough solution to cover the sample (3–5 drops per sample) and incubate for 8min, gently tilt the plate from time to time.
    d. Add 1mL ddH_2O to stop the reaction.
5. Wash with ddH_2O thoroughly, 6×10min @RT.
6. Check under a light microscope with bright field, positive signal should show dark brown color (Fig. 3B) with clearly positive signal (Fig. 3C), only process those promising specimens.

Pause Point: (sample can be stored in ddH_2O overnight at 4°C.)

Note:

1. All washing steps were performed on an Orbital shaker at low speed (set as 2).
2. Silver enhancement kit stored at −20°C in dark. Take the bottles out of the freezer and leave it in a dark room at least 2h before the silver enhancement

reaction, to make sure that all solutions are warmed up to room temperature before using it.

3. Silver enhancement should be performed in a dark room with safety red light. Items required for this procedure need to be brought into dark room before the silver enhancement step: Timer to set at 8min, 2mL or 5mL Eppendorf tubes for mixing the solution, 1mL pipet with tip for adding ddH_2O to stop the reaction, disposable plastic transfer pipet for adding mixed solution on sample well, and ddH_2O in 50mL falcon tube.

4. Add equal drops of A, B and C into a 2mL, or 5mL Eppendorf tube depending the total final volume needed. A 2mL Eppendorf tube would contain 15 drops of each A, B, and C, which is enough reagent for a total of six sections. Solution B is stickier and less fluid, make sure to hold the bottle vertical when squeezing the desired volume out of the bottle.

5. Wash the sample with 0.02M sodium citrate buffer before silver enhancement might reduce the labeling background.

7 Critical: Stable room temperature and fixed silver developing time is essential for the reproducibility of the experimental results

The silver enhancement reaction time and room temperature affect the growth of gold particles. Therefore, a stable room temperature and proper time control after applying the solution to the sample is important for the reproducibility of the experimental results. When the room temperature is set at 25°C, an 8–10min reaction time will generate 20–30nm silver coated gold particles. It is essential to wash the samples thoroughly with ddH_2O before the silver enhancement, because the buffer used for antibody incubation, washing and fixation contains chloride ions. Other anions might form insoluble precipitates with silver, which are often light-sensitive and will give non-specific staining. It is also important to wash the sample vigorously after silver enhancement, to stabilize the silver structure. Otherwise, uranyl acetate block staining might dissolve the silver particles, leading to empty spaces around the silver particles. An overnight water washing step at 4°C, or gold toning step after silver enhancement (to add a layer of gold on top of silver) would overcome the silver quench issue (Sawada & Esaki, 1994).

7.1 EM processing and resin embedding

Timing: ~5h plus 8h infiltration and 48h polymerization

1. Wash with ddH_2O, 2×15min, on ice
2. Osmication with 0.5% OsO_4 15min, on ice
3. Wash with ddH_2O 3×5min, on ice
4. Block stain with 0.5% UA 60min in the dark @4°C
5. Wash with ddH_2O 4×5min, on ice.
6. Dehydration with 30% ethanol, 5min, on ice.

7. Dehydration with 50% ethanol, 5min, on ice.
8. Dehydration with 70% ethanol, 5min, on ice.
9. Dehydration with 85% ethanol, 5min, @RT.
10. Dehydration with 95% ethanol, 5min, @RT.
11. Dehydration with 100% ethanol, 2×5min, @RT.
12. Dehydration with 100% acetone, 2×5min, @RT.
13. Infiltration with acetone: Epon w/o BDMA mix 1:1 @RT, 4h.
14. Infiltration with acetone: Epon w/o BDMA mix 1:2 overnight @RT.
15. Infiltration with Epon w/o BDMA 2×2h @RT.
16. Infiltration with Epon w/ BDMA 2×2h @RT.
17. Embed by sandwiching between two sheets of ACLAR film and glass slide (Fig. 4A and B).
18. Polymerization, 48h, @60°C oven.

Note:

1. All washing steps were performed on an Orbital shaker at low speed (set as 2).
2. Low temperature dehydration will better preserve the cell membrane structure.
3. Change the sample from a 24 wells plate to a 5mL Eppendorf tube or glass scintillation vails in70% ethanol,because acetone and Epon willdissolvetheplate.
4. Either hard Epon or Durcupan can be used for embedding (Table 1). Put ACLAR film on top of the glass slide, and put the sample flat on the ACLAR sheet. Add one drop of resin on top of each sample, and put the sample number on the side, then put another layer of ACLAR film on top of the sample and slowly lower the ACLAR film to avoid air bubbles. Add another glass slide on top of the ACLAR sheets, the extra weight of glass slide might avoid air bubbles between ACLAR sheets (Fig. 4A and B). The glass slide-ACLAR-sample-ACLAR-glass slide sandwich should be contained on a piece of aluminum foil with the sides folded up, to avoid resin drip in the oven.
5. For polymerization, shelves inside the oven should be properly balanced to avoid uneven distribution of the resin.

7.2 Sample mounting

Timing: ~3h

1. Separate the glass slide from the ACLAR sheets using a razor blade.
2. Remove the sample from the ACLAR film (Fig. 4C).
3. Identify the regions of interest (ROIs), left ventricle (LV) and right ventricle (RV). Cut out the ROIs using a razor blade (Fig. 4D).

4. Glue the sample pieces flat on layered 3View pins (Fig. 4E) using conductive silver epoxy (Denk & Horstmann, 2004; Starborg et al., 2013). A base layer of silver epoxy helps to electrically ground the tissue block. Allow the silver epoxy, 3View SEM pin and sample to fully polymerize via overnight incubation at 60°C.

5. Place the 3View pin into the specimen arc of the ultramicrotome, and ensure both specimen arc and knife holder are at zero degrees.

6. Trim two sample sides parallel to each other using a razor. The other two sides can be trimmed to define a square or a rectangle. The block-face should be trimmed such that it is no longer than 1.0mm in either dimension. The block should resemble a trapezoidal frustum.

7. Use a glass knife or a Diatome histo diamond knife to smoothen the sample surface at 500nm section thickness at a speed of 1mm/s.

8. Collect one 70nm thin section onto a slotted grid and image under TEM to check the quality of the immunolabeling (Fig. 5A and B).

9. Coat the 3View pin with a thin layer (15nm) of gold with a sputter coater to further enhance the conductivity of the sample block. The mirror-finish of the block-face will also help with approaching the sample to the cutting plane of the 3View microtome.

10. Heat the sample in an oven set to 100°C for one hour to improve the cutting performance of the sample embedding resin during SBF-SEM imaging.

7.3 Optional steps

Silver paint can be applied to the sides of the sample block before sputter coating to further improve conductivity. This is useful for thicker non-conductive samples which are more susceptible to sample charging artifacts during SEM imaging.

Note:

1. Cutting the ROIs from the sample must be done very careful to ensure that the samples are not lost. Use a piece of white paper as background. A piece of scotch or other pressure-adhesive tape placed under the sample block may help prevent small pieces from being lost.

2. The platform of the 3View pin should have a layer of conductive silver epoxy which acts as an electrical contact between the tissue and metal. Once the epoxy is placed onto the pin, it should be polymerized overnight in an oven set to 60°C. It is important to make the epoxy layer flat so that the final sample will be parallel to the surface.

3. Due to the fixed angle of the diamond knife in SBF-SEM, the surface of the sample should be parallel to the stub surface, so that the image will be in focus over the entire sample face.

4. The sputter coating thickness for the sample/3View pin can range from 5 to 15nm. Either gold or 80/20 gold/palladium can be used for coating. There may be diminishing returns beyond certain thicknesses.

7.4 Image acquisition

Timing: 12–15h

1. Place the 3View pin with sample into the 3View microtome chunk and secure it by tightening a set screw. Under a stereo microscope, adjust the concentric adjustment pedestals on the chuck to center the tissue to the middle of the chuck.
2. Load the chunk with sample into the 3View microtome.
3. Shift the diamond knife laterally and adjust the cutting window position to center over the span of the block face. Note that the cutting window is 1.2mm. Make sure that the base of the sample block is no larger than 1.2mm in either width or length.
4. In Digital Micrograph, make sure that the chuck is in the raised position—this is the elevated state that the block will be in during each cutting cycle. It will be in the lowered state when the knife cycles back to the start of the cutting window, preventing the knife from colliding with the block.
5. Manually approach the sample surface to the diamond knife using the stereoscope, which can be mounted to the 3View door. An LED light is used to illuminate the block face and aid in the sample approach, similar to classical ultramicrotomy.
6. A practiced user should be able to manually approach within 5–8μm of the cutting plane. Once approached, use Sample Approach in Digital Micrograph to automatically approach the rest of the way. Set the section thickness to 100nm and the number of cuts between 25 and 100. Monitor the block surface with the stereoscope. Stop approaching when you see that the knife has started to cut the surface—this includes partial cuts of the block-face. Once approached, adjust the position of the FCC needle such that it is as close as possible to the edge of the block. The needle should be vertically positioned such that the nitrogen gas blows over the block-face.
7. Close the chamber and pump down the microscope. The remainder of the imaging steps are done in software.
8. With the high-tension on and set to 1.2–2.0kV, obtain a live image using the Gatan BSE OnPoint detector and center the block-face. The magnification should be low enough such that it captures the entire block-face.
9. Run the Sample Approach again, this time ensuring that the knife oscillator is on and the number of sections to cut is set to 5–25 slices. This is to ensure that the block-face is still in the cutting plane after the microtome is pumped down to vacuum. Compare the surface of the block before and after to confirm it is in plane with the knife.

10. Set the chamber pressure, working distance and electron beam settings as well as the data acquisition settings shown in Table 2.

11. In SmartSEM (Carl Zeiss GmbH), select the secondary electron detector, activate Beam Wobble and adjust the aperture X and Y position to center and align the mid-lens aperture. Deactivate Beam Wobble once the aperture is aligned.

12. Create and position an imaging tile (or tile-set) over gold labeled gap junction regions.

13. Enter the image tags in the Global Info settings with information such as sample name, lab name, sample block number (if applicable), embedding resin used, aperture size and FCC pressure. Imaging parameters such as slice thickness, pixel size, dwell time and acceleration voltage are automatically embedded in the metadata.

14. Assign a storage directory for the saved dataset. Each scan is saved as an individual file in the native Gatan Digital Micrograph ".dm4" file format. Multiple regions of interest are saved into their respective folders (ROI_00, ROI_01, et cetera).

15. Start image acquisition by pressing in the bottom right panel of the Digital Micrograph software (Fig. 6).

16. For a multiple ROI dataset collection, confirm the positions of the ROIs and assign a region as a "monitor stack," which allows for the storage of several sequential scans in RAM for quick viewing. This is used to monitor cutting quality, sample charge rate and to perform any focus corrections during data collection.

17. Make any focus and stigmation corrections after the first image is acquired. Monitor the first few scans to assess cutting quality and to spot any charging artifacts in the image. Increase the FCC pressure to compensate for sample charge.

18. Monitor imaging periodically onsite or remotely with remote accessing software to manually correct for any focus drift that may occur during acquisition.

19. For the nanogold labeled sample: image frames were set to 38×50μm in XY, and 50nm thickness in Z. Stacks of 150 slices were aligned using the slices registration tool in ORS Dragonfly (Object Research Systems Inc.). A total volume of $38\times50\times15\mu m^3$ was obtained from the tissue block in each dataset (van Opbergen et al., 2022). The same parameters were used for collecting FNG labeled sample (Table 2).

Note:

1. The accelerating voltage can be set between 1.2 – 2 keV depending on the conductivity and charge tolerance of the sample. Higher accelerating voltages allow for better image resolution. However, the likelihood and severity of charging artifacts will also be greater.

2. Avoid bumping the block face into the knife edge when approaching the cutting plane. This might not only damage the knife but also leave an imprint in the block-face that can be many microns deep. These imprints can negatively affect cutting and imaging quality.
3. The proximity of the FCC needle greatly affects the efficacy of charge reduction. The relationship between distance and magnetic field strength is an inverse-cube.
4. Typical 3View imaging workflows have one low mag large imaging area plus two higher-resolution smaller ROIs acquired simultaneously. Number of ROIs and their sizes is limited by the amount of RAM available on the computer. Images are stored in memory in a data buffer before being written to their designated directories.
5. Higher FCC pressures can negatively impact the signal-to-noise and contrast of the datasets. It is best practice to find the minimum percentage necessary to avoid charging artifacts.
6. 3View data collection typically runs for at least 6h. Therefore, remote access to the microscope computer is essential to monitor and correct focus drift while the user is away from the lab.

7.5 Imaging data processing

Timing: ~15 days

1. Convert images from .dm3 format to .tif. Batch conversion can be done in either Digital Micrograph or using ImageJ.
2. Converted datasets are loaded into ImageJ for initial brightness and contrast adjustments. Datasets are typically converted from 16- bits to 8-bits to reduce file sizes and streamline processing later in the pipeline.
3. A two-pixel Gaussian blur is applied to the datasets to improve the signal-to-noise of the images. This improves image clarity and aids segmentation of sample structures via intensity thresholding (Fig. 7).
4. Processed datasets are imported into ORS Dragonfly for alignment and segmentation.
5. A segmentation layer is created per structure of interest. The Brush tool was used to highlight structures where intensity-based thresholding would be insufficient or inaccurate.
6. After segmentation, a vertex-based 3D mesh is generated that represents the highlighted structures as a contiguous shape. Laplacian smoothing is then applied to the mesh.
7. The mesh, along with original dataset stack, are shown in 3D and a movie is generated (Supporting Information Movie 1 in the online version at https://doi.org/10.1016/bs.mcb.2022.12.020). Rotations around a fixed axis help illustrate morphological features or show associations of adjacent structures.

8 Expected outcomes

FNG labeled cardiac vibratome sections can be visualized under fluorescence microscope (van Opbergen et al., 2022), serving as a reference for correlative microscopy. Both NG and FNG labeled vibratome sections show after silver enhancement distinctly dark brown color lines or dots, under the bright-field light microscope (Fig. 3B and C). Negative control samples in which the primary antibody was omitted, show a unified light brown color, without a specific lined or dotted pattern (data not shown). The entire vibratome section will turn dark and no specific signal can be detected after osmification (Fig. 4B–D).

Fig. 5 shows typical results for the labeling of Cx43 using pre-embedding vIEM in wild type cardiac sections, samples were imaged using TEM. Gold labelled Cx43 was distinctly visible in the perinexus of the gap junction plaque. Mitochondria (M) were well preserved with clearly defined crista, as well were muscle fibers (MF) and Z bands (Z). The intercalated disc (ID) was easily to be visualized at low magnification because of the gold labelled gap junctions (G), though desmosomes (D) and adherens junctions (AJ) could be clearly defined as well.

Fig. 8 shows the partially exposed sample surface at the beginning of SBF imaging. Gold particle labeled Cx43 can be clearly defined on gap junction plaques (Fig. 8A), even on incomplete imaging. These pictures can be used to define the ROI for future data collection. Fig. 8B shows the nanogold signal at slice 226 in the collected ROI. During serial image data collection in a Z-range of 15 μm depth, the ID orientation and morphology largely changes in the X and Y direction (Fig. 8A and B). Therefore, it is necessary to set up a larger ROI (~XY=30×50μm) to catch the entire ID structure. 3D segmentation of reconstructed images allowed us to visualize closely packed strings of Cx43-gold particles on the entire length of two parallel gap junction plaques at the ID (Fig. 9). Bulging of the intercellular space and areas where only one of two strings of Cx43-immunoreactive beads were present became apparent in the PKP2cKO cardiac samples. These Cx43-gold particles were lacking opposing gold particles in close proximity, indicating the presence of orphan Cx43 hemichannels in adult PKP2cKO murine hearts (van Opbergen et al., 2022).

9 Quantification and statistical analysis

Detailed analysis for both the RV and LV images in control and PKP2cKO cardiac samples was performed. As mentioned above, separation of closely aligned Cx43 beads became apparent in the PKP2cKO cardiac samples, in both the left and right ventricular free wall. This showed an average 1.5x increase in 2D surface and maximal width between ID membranes. In addition, we also observed gap junction plaques that, for some length, showed only one single strand of Cx43 immunoreactive beads (Cx43 hemiplaques). Cx43 hemiplaques were present in both ventricular walls of PKP2cKO hearts, but to a higher extent in the RV. In addition, the data showed that the total length of Cx43 hemiplaques in the RV was over three times longer in PKP2cKO than in control hearts, or in the LV of either control or PKP2cKO hearts (van Opbergen et al., 2022). Details on data and statistical analysis are described in van Opbergen et al., 2022.

10 Advantages

This method is primarily developed for cardiac vibratome sections, though it is applicable to 3D imaging of protein localization in several animal tissue types, considering some modifications on the sample permeabilization steps. The very small nanogold (1.4nm) clusters allow efficient penetration (~40μm) inside fixed tissues prior to sample embedding (Robinson & Vandre, 1997), which is ideal for high resolution 3D imaging. Our experiments show that both NG and FNG could easily penetrate into at least 20μm depth on both sides of the cardiac vibratome sections, after Triton X-100 treatment, which provides enough 3D volume to study prime cellular events.

Volume imaging of biological samples, making use of SEM, is often hampered by sample charging and typically requires specific sample preparation. For example, the implementation of heavy mental stains such as an intensive osmium reaction, plus extended uranium and lead staining before embedding. These steps are performed in order to increase the conductivity of the sample and reduce the charging during SEM imaging. Those en bloc stains can also increase the image contrast. However, darker staining of the tissue makes gold particles harder to distinguish in IEM images, in contrast to the cellular structures. In this protocol, we only applied a low percentage of heavy metal staining, such as 0.5% osmium tetroxide for 15min, and 0.5% uranyl acetate for one hour, to avoid a too dark labeling of the cellular structures. To overcome charge issues during SBF imaging, caused by the absence of heavy metals in the staining protocol, recruiting silver enhanced gold particles inside the sample greatly improved conductivity of the sample. Therefore, it partially worked as a sample embedding agent in conductive resin (Nguyen et al., 2016), which greatly reduced sample charging during SBF imaging.

As an immunoprobe, FNG consists of a gold cluster compound covalently linked to a fluorochrome-labeled antibody (Takizawa & Robinson, 2000a, 2000b). The fluorescent FNG signal can be detected at first by fluorescence microscopy, after which the gold signal can be recorded by electron microscopy due to silver enhancement of the sample. This provides a great opportunity for general use in correlative microscopy (Robinson & Vandre, 1997; Takizawa & Robinson, 2000b). This protocol not only enables visualization of the ID morphology and separation of the ID membranes, but also the presence of orphan hemichannels and asymmetric gap junctions, by labeling with gold particles (van Opbergen et al., 2022). These data represent a step forward in the development of novel methodologies for visualization of specific protein aggregates in native tissue, at nanometric resolution and in three dimension by various kinds of volume microscopy.

11 Limitations

The limitation of this protocol is that this protocol does not facilitate to study colocalization of two or more antigens. However, switching from the use of nanogold to ultrasmall gold particles might partially work for double immunolabeling (Yi, Leunissen, Shi, Gutekunst, & Hersch, 2001). Using Triton X-100 as a permeabilization reagent after aldehyde fixation does not cause visible ultrastructural damage in tissue samples, for example the heart and brain (unpublished). However, the plasma membrane of *in vitro* cultured cells is quite

sensitive to Triton X-100. Coupling cell pellets with frozen sections can potentially be used as an alternative method for the permeabilization of *in vitro* cultured cells (Melo et al., 2014).

12 Safety Considerations and Standards

Details of relevant safety considerations and international or national safety standards/regulations to be considered.

1. Fume hood and proper gloves are essential in the electron microscopy lab since most chemicals are toxic, irritated to skin and eye, and some are known carcinogens.
2. Paraformaldehyde, glutaraldehyde, osmium tetroxide and epoxy resins are toxic, irritant to eyes and skin. Therefore, the reagents should only be used in a fume hood and handled with gloves. Dry milk can be used to contain the wasted aldehyde, while osmium tetroxide can be kept in a waste bottle filled half full with core oil, after which it should be disposed as chemical waste. The waste of epoxy resins can be polymerized in 60°C and disposed as regular lab trash.
3. Uranyl acetate is toxic and slightly radioactive, it should be handled with gloves and disposed according the national safety guideline.
4. Ethanol and acetone are flammable and toxic upon inhalation, should be used in the fume hood and disposed as chemical waste.

Supplementary Material

Refer to Web version on PubMed Central for supplementary material.

Acknowledgments

We thank Mark Alu for his assistance for generating vibratome sections, and Kristen Dancel-Manning for her assistance with the illustrations. Microscopy Laboratory is partially supported by Laura and Isaac Perlmutter Center Support Grant NIH/NCI P30CA016087. Zeiss Gemini300 SEM with 3View was purchased with NIH S10 OD019974. This work was also supported by NIH grants RO1-HL134328, RO1-HL136179 and RO1-HL145911 (MC), a Transatlantic Network of Excellence from the Leducq Foundation (MD), the Wilton W. Webster Followship in Pediatric Electrophysiology from Heart Rhythm Society, and an American Heart Association Postdoctoral Fellowship (CvO).

References

Baschong W, & Stierhof YD (1998). Preparation, use, and enlargement of ultrasmall gold particles in immunoelectron microscopy. Microscopy Research and Technique, 42(1), 66–79. 10.1002/(SICI)1097-0029(19980701)42:1<66::AID-JEMT8>3.0.CO;2-P [PubMed: 9712164]

Cerrone M, Noorman M, Lin X, Chkourko H, Liang FX, van der Nagel R, et al. (2012). Sodium current deficit and arrhythmogenesis in a murine model of plakophilin-2 haploinsufficiency. Cardiovascular Research, 95(4), 460–468. 10.1093/cvr/cvs218. [PubMed: 22764151]

Cheutin T, Sauvage C, Tchelidze P, O'Donohue MF, Kaplan H, Beorchia A, et al. (2007). Visualizing macromolecules with fluoronanogold: from photon microscopy to electron tomography. Methods in Cell Biology, 79, 559–574. 10.1016/S0091-679X(06)79022-7. [PubMed: 17327174]

Delmar M, & Liang FX (2012). Connexin43 and the regulation of intercalated disc function. Heart Rhythm, 9(5), 835–838. 10.1016/j.hrthm.2011.10.028. [PubMed: 22056332]

Denk W, & Horstmann H (2004). Serial block-face scanning electron microscopy to reconstruct three-dimensional tissue nanostructure. PLoS Biology, 2(11), e329. 10.1371/journal.pbio.0020329. [PubMed: 15514700]

Faulk WP, & Taylor GM (1971). An immunocolloid method for the electron microscope. Immunochemistry, 8(11), 1081–1083. 10.1016/0019-2791(71)90496-4. [PubMed: 4110101]

Gerull B, Heuser A, Wichter T, Paul M, Basson CT, McDermott DA, et al. (2004). Mutations in the desmosomal protein plakophilin-2 are common in arrhythmogenic right ventricular cardiomyopathy. Nature Genetics, 36(11), 1162–1164. 10.1038/ng1461. [PubMed: 15489853]

Giepmans BN (2008). Bridging fluorescence microscopy and electron microscopy. Histochemistry and Cell Biology, 130(2), 211–217. 10.1007/s00418-008-0460-5. [PubMed: 18575880]

Griffiths G (1993). Fine structure immunocytochemistry. Berlin/Heidelberg/New York: Springer-Verlag.

Grossmann KS, Grund C, Huelsken J, Behrend M, Erdmann B, Franke WW, et al. (2004). Requirement of plakophilin 2 for heart morphogenesis and cardiac junction formation. The Journal of Cell Biology, 167(1), 149–160. 10.1083/jcb.200402096. [PubMed: 15479741]

Hagiwara H, Aoki T, Suzuki T, & Takata K (2010). Pre-embedding immunoelectron microscopy of chemically fixed mammalian tissue culture cells. Methods in Molecular Biology, 657, 145–154. 10.1007/978-1-60761-783-9_11. [PubMed: 20602213]

Hainfeld JF, & Furuya FR (1992). A 1.4-nm gold cluster covalently attached to antibodies improves immunolabeling. The Journal of Histochemistry and Cytochemistry, 40(2), 177–184. 10.1177/40.2.1552162. [PubMed: 1552162]

Jimenez N, & Post JA (2012). A novel approach for intracellular 3D immuno-labeling for electron tomography. Traffic, 13(7), 926–933. 10.1111/j.1600-0854.2012.01363.x. [PubMed: 22486935]

Kerr DE, Liang F, Bondioli KR, Zhao H, Kreibich G, Wall RJ, et al. (1998). The bladder as a bioreactor: Urothelium production and secretion of growth hormone into urine. Nature Biotechnology, 16(1), 75–79. 10.1038/nbt0198-75.

Kim JC, Perez-Hernandez M, Alvarado FJ, Maurya SR, Montnach J, Yin Y, et al. (2019). Disruption of Ca(2+)i homeostasis and connexin 43 hemichannel function in the right ventricle precedes overt arrhythmogenic cardiomyopathy in plakophilin-2-deficient mice. Circulation, 140(12), 1015–1030. 10.1161/CIRCULATIONAHA.119.039710. [PubMed: 31315456]

Koster AJ, & Klumperman J (2003). Electron microscopy in cell biology: Integrating structure and function. Nature Reviews. Molecular Cell Biology, Suppl, SS6–S10. Retrieved from https://www.ncbi.nlm.nih.gov/pubmed/14587520. [PubMed: 14587520]

Lam SS, Martell JD, Kamer KJ, Deerinck TJ, Ellisman MH, Mootha VK, et al. (2015). Directed evolution of APEX2 for electron microscopy and proximity labeling. Nature Methods, 12(1), 51–54. 10.1038/nmeth.3179. [PubMed: 25419960]

Leo-Macias A, Agullo-Pascual E, Sanchez-Alonso JL, Keegan S, Lin X, Arcos T, et al. (2016a). Erratum: Nanoscale visualization of functional adhesion/excitability nodes at the intercalated disc. Nature Communications, 7, 10919. 10.1038/ncomms10919.

Leo-Macias A, Agullo-Pascual E, Sanchez-Alonso JL, Keegan S, Lin X, Arcos T, et al. (2016b). Nanoscale visualization of functional adhesion/excitability nodes at theintercalated disc. Nature Communications, 7, 10342. 10.1038/ncomms10342.

Leo-Macias A, Liang FX, & Delmar M (2015). Ultrastructure of the intercellular space in adult murine ventricle revealed by quantitative tomographic electron microscopy. Cardiovascular Research, 107(4), 442–452. 10.1093/cvr/cvv182. [PubMed: 26113266]

Liang FX, Bosland MC, Huang H, Romih R, Baptiste S, Deng FM, et al. (2005). Cellular basis of urothelial squamous metaplasia: Roles of lineage heterogeneity and cell replacement. The Journal of Cell Biology, 171(5), 835–844. 10.1083/jcb.200505035. [PubMed: 16330712]

Liang FX, Petzold C, Dancel-Manning K, Sall J, Ren P, & Zhou C (2021). Challenges facing an EM core laboratory: Mitochondria structural preservation and 3DEM data presentation. Microscopy Today, 29(1), 6. 10.1017/S1551929520001777.

Martell JD, Deerinck TJ, Sancak Y, Poulos TL, Mootha VK, Sosinsky GE, et al. (2012). Engineered ascorbate peroxidase as a genetically encoded reporter for electron microscopy. Nature Biotechnology, 30(11), 1143–1148. 10.1038/nbt.2375.

Melo RC, Morgan E, Monahan-Earley R, Dvorak AM, & Weller PF (2014). Preembedding immunogold labeling to optimize protein localization at subcellular compartments and membrane microdomains of leukocytes. Nature Protocols, 9(10), 2382–2394. 10.1038/nprot.2014.163. [PubMed: 25211515]

Newman GR, & Hobot JA (1993). Resin microscopy and on-section immunocytochemistry. Berlin Heidelberg: Springer-Verlag.

Nguyen HB, Thai TQ, Saitoh S, Wu B, Saitoh Y, Shimo S, et al. (2016). Conductive resins improve charging and resolution of acquired images in electron microscopic volume imaging. Scientific Reports, 6, 23721. 10.1038/srep23721. [PubMed: 27020327]

Peddie CJ, Genoud C, Kreshuk A, Meechan K, Micheva KD, Narayan K, et al. (2022). Volume electron microscopy. Nature Reviews Methods Primers, 2(1), 51. 10.1038/s43586-022-00131-9.

Perkins GA (2014). The use of miniSOG in the localization of mitochondrial proteins. Methods in Enzymology, 547, 165–179. 10.1016/B978-0-12-801415-8.00010-2. [PubMed: 25416358]

Robinson JM, & Vandre DD (1997). Efficient immunocytochemical labeling of leukocyte microtubules with FluoroNanogold: An important tool for correlative microscopy. The Journal of Histochemistry and Cytochemistry, 45(5), 631–642. 10.1177/002215549704500501. [PubMed: 9154150]

Roth J, Bendayan M, & Orci L (1978). Ultrastructural localization of intracellular antigens by the use of protein A-gold complex. The Journal of Histochemistry and Cytochemistry, 26(12), 1074–1081. 10.1177/26.12.366014. [PubMed: 366014]

Sabatini DD, Bensch K, & Barrnett RJ (1963). Cytochemistry and electron microscopy. The preservation of cellular ultrastructure and enzymatic activity by aldehyde fixation. The Journal of Cell Biology, 17, 19–58. 10.1083/jcb.17.1.19. [PubMed: 13975866]

Sawada H, & Esaki M (1994). Use of nanogold followed by silver enhancement and gold toning for preembedding immunolocalization in osmium-fixed, Epon-embedded tissues. Journal of Electron Microscopy (Tokyo), 43(6), 361–366. Retrieved from https://www.ncbi.nlm.nih.gov/pubmed/7722428.

Seveus M, Vaisala M, Kojola H, Roomans GM, & Soini E (1994). Use of fluorescent Europium chelates as labels in microscopy allows glutaraldehyde fixation and permanent mounting and leads to reduced autofluorescence and good long-term stability. Microscopy Research and Technique, 28, 5.

Shu X, Lev-Ram V, Deerinck TJ, Qi Y, Ramko EB, Davidson MW, et al. (2011). A genetically encoded tag for correlated light and electron microscopy of intact cells, tissues, and organisms. PLoS Biology, 9(4), e1001041. 10.1371/journal.pbio.1001041. [PubMed: 21483721]

Starborg T, Kalson NS, Lu Y, Mironov A, Cootes TF, Holmes DF, et al. (2013). Using transmission electron microscopy and 3View to determine collagen fibril size and three-dimensional organization. Nature Protocols, 8(7), 1433–1448. 10.1038/nprot.2013.086. [PubMed: 23807286]

Takizawa T, & Robinson JM (2000a). Analysis of antiphotobleaching reagents for use with FluoroNanogold in correlative microscopy. The Journal of Histochemistry and Cytochemistry, 48(3), 433–436. 10.1177/002215540004800313. [PubMed: 10681397]

Takizawa T, & Robinson JM (2000b). FluoroNanogold is a bifunctional immunoprobe for correlative fluorescence and electron microscopy. The Journal of Histochemistry and Cytochemistry, 48(4), 481–486. 10.1177/002215540004800405. [PubMed: 10727289]

van Opbergen CJM, Sall J, Petzold C, Dancel-Manning K, Delmar M, & Liang FX (2022). “Orphan” connexin43 in plakophilin-2 deficient hearts revealed by volume electron microscopy. Frontiers in Cell and Development Biology, 10, 843687. 10.3389/fcell.2022.843687.

Yi H, Leunissen J, Shi G, Gutekunst C, & Hersch S (2001). A novel procedure for pre-embedding double immunogold-silver labeling at the ultrastructural level. The Journal of Histochemistry and Cytochemistry, 49(3), 279–284. 10.1177/002215540104900301. [PubMed: 11181730]

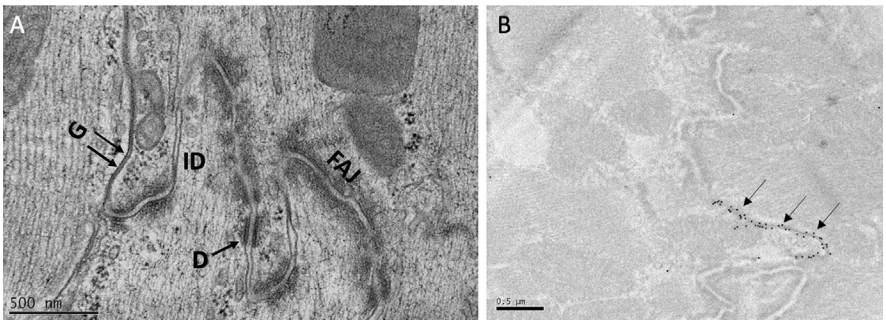

FIG. 1.

Intercalated disc morphology and Cx43 localization in murine cardiac tissue. (A) Murine heart tissue prepared by high pressure freezing and freeze substitution shows a well-preserved intercalated disc (ID) morphology, consisting of gap junctions (G), desmosomes (D) and fascia adherens junctions (FAJ). (B) Clear labeling of Cx43 at gap junctions by 15nm gold particles on Lowicryl K4M embedded murine heart tissue. The structure of desmosomes and adherens junctions is not well defined in Lowicryl embedded samples.

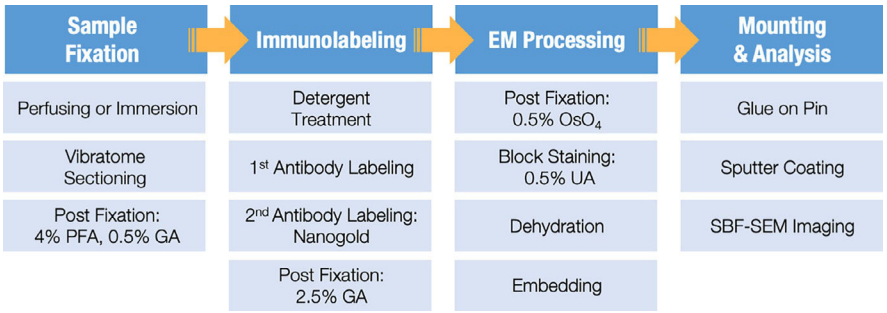

FIG. 2.

Workflow of the pre-embedding volume immunogold electron microscopy (vIEM) procedure.

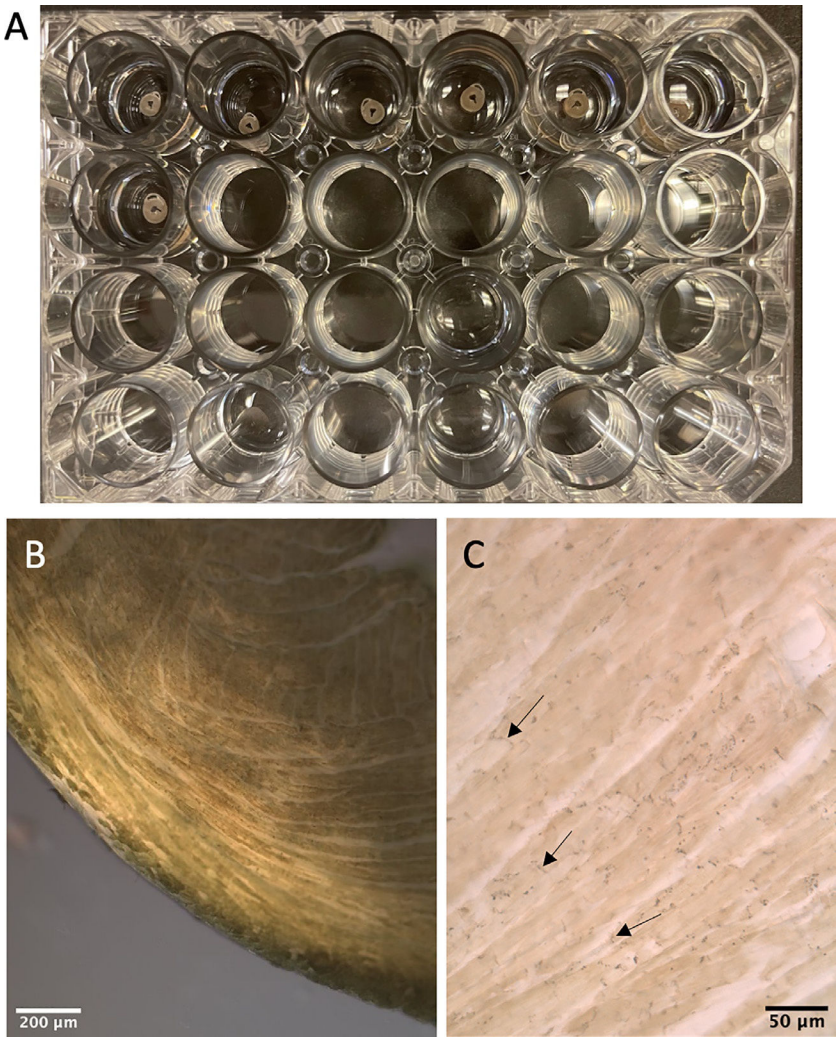

FIG. 3.

Pre-embedding immunogold labeling of murine cardiac tissue with silver enhancement. (A) Thick cross sections of 200µm thickness from murine hearts preserved in 4% PFA, stored in a 24-well plate, and sectioned with a vibratome. (B) Low magnification nanogold visualization after silver enhancement of Cx43 by light microscopy in adult murine cardiac sections. The Cx43-nanogold labeled section shows brownish labeling after silver enhancement, presenting darker lines or dots as positive signal. (C) Zoom-in of nanogold labeling after silver enhancement by light microscopy demonstrating in more detail the expression pattern of Cx43 in the cardiac sample. Gap junctions are highlighted by the arrow heads.

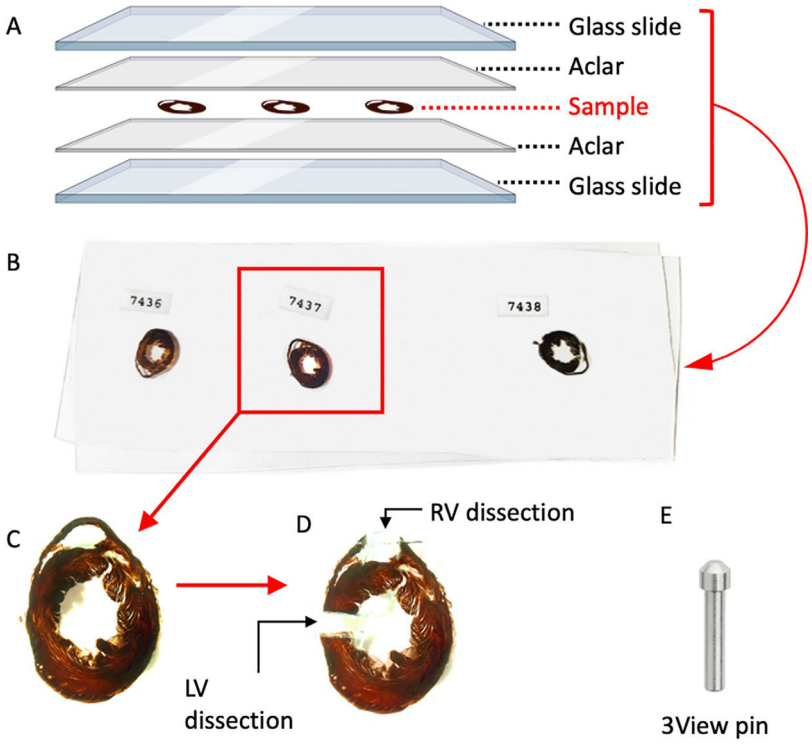

FIG. 4.

Workflow of cardiac tissue sample embedding, dissection and mounting for SBF-SEM imaging. Murine cardiac muscle cross sections were flat embedded between ACLAR film and glass slides (A), and polymerized at 60°C in the oven (B). The entire cross section (B and C) shows a dark brownish labeling and sample numbers are indicated on top. Small LV and RV areas were manually dissected and mounted on a 3View pin (E). LV: left ventricle, RV: right ventricle.

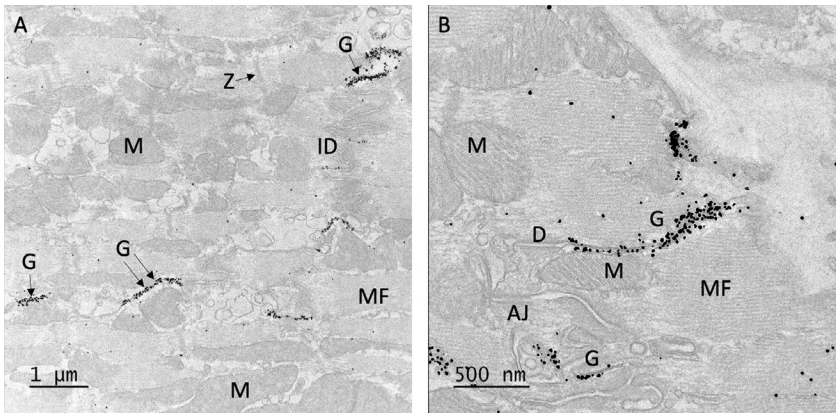

FIG. 5.

Specific Cx43 visualization in gap junctions of adult murine hearts by nanogold labeling after silver enhancement. Cardiac vibratome cross sections fixed in 4% PFA were immunolabelled for Cx43, coupled with nanogold, and treated with silver enhancement. TEM images of thin cardiac sections illustrate the distribution of Cx43 in the murine heart. Gold particles are specifically lined on the membrane of gap junctions (G), this can be observed at low magnification (A) and high magnification (B). The primary antibody is anti-Connexin 43 rabbit polyclonal antibody (1:50 dilution, Millipore Sigma), and secondary antibody is Nanogold Fab' anti-rabbit conjugated (1:200 dilution, Nanoprobes, Cat. # 2004).

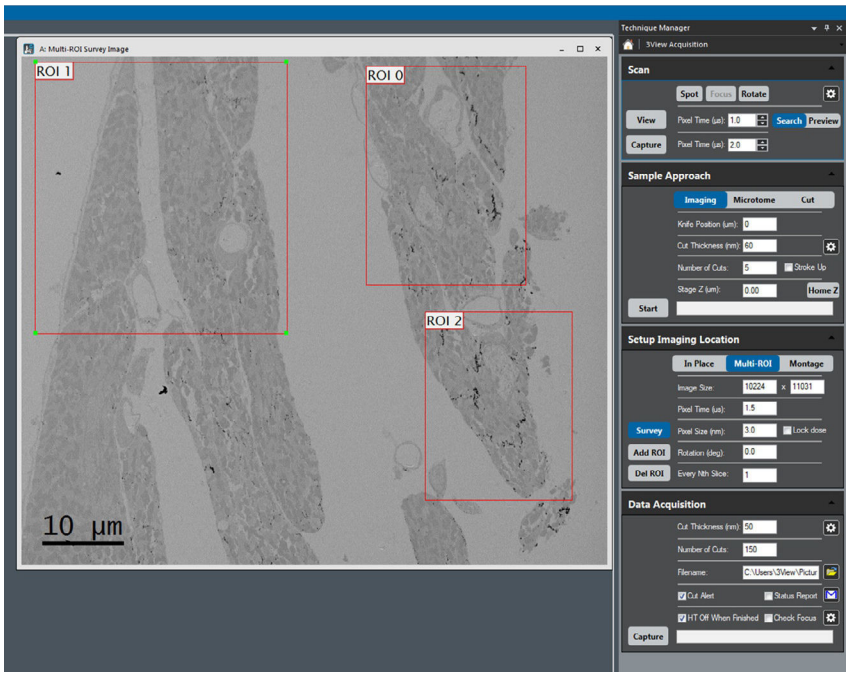

FIG. 6.

SBF-SEM imaging parameters used for 3View data collection with Gatan Digital Micrograph.

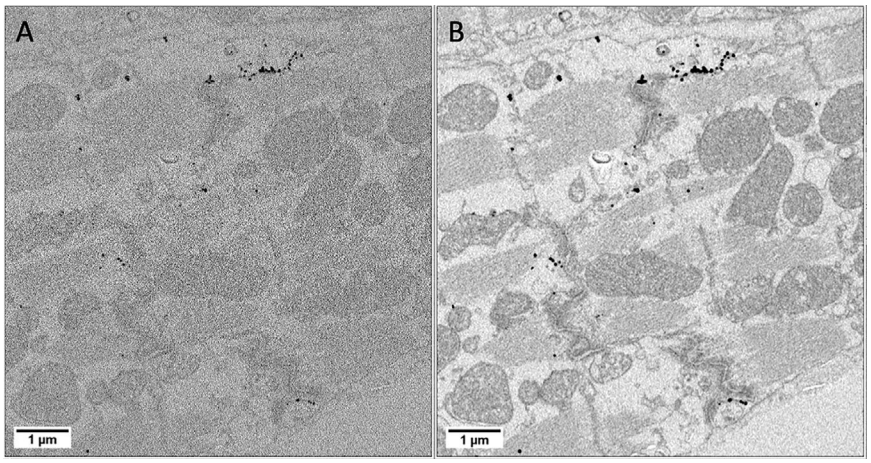

FIG. 7.

SBF-SEM image processing. (A) Original unprocessed image. (B) 2—pixel gaussian blur is applied to improve the signal-to-noise ratio of the image. Note that there was no contrast adjustment applied after the gaussian blur.

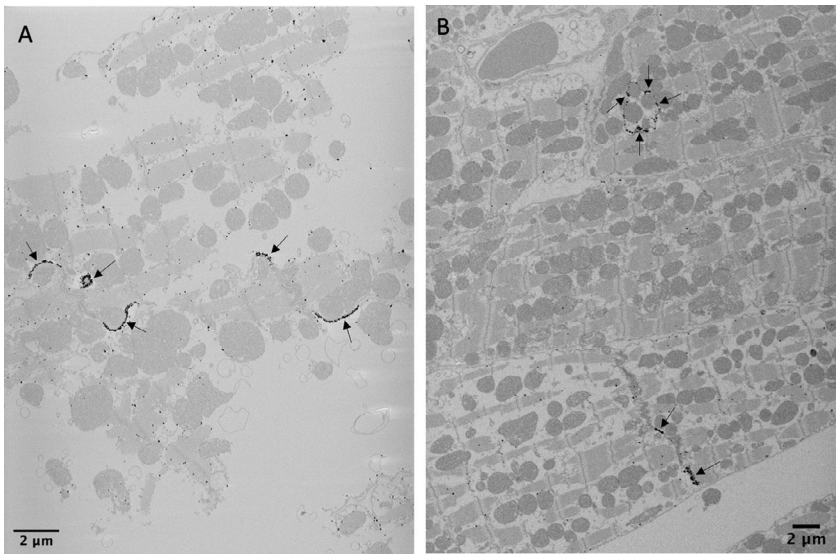

FIG. 8.

SBF-SEM imaging data collection. (A) The first imaging plane of the sample shows an incomplete section, though there is already clear positive labeling visible in the image. (B) At slice 236 after sectioning, through at ~12μm deep into the sample, the entire tissue morphology is visible and gold particle-labeled structures are still detectable in sample.

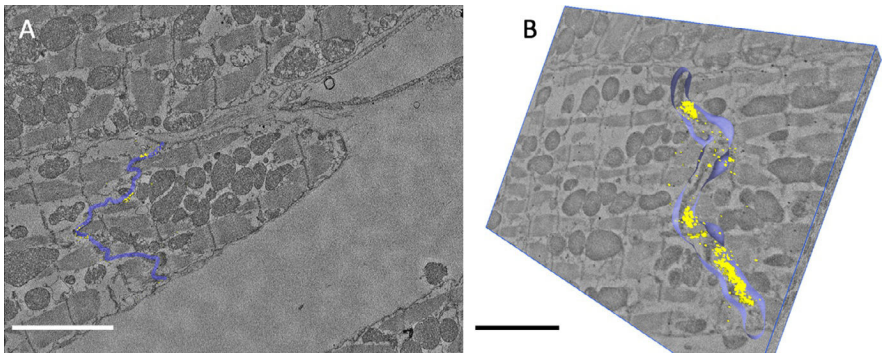

FIG. 9.

Three-dimensional segmentation of the intercalated disc (ID) performed by use of corresponding Cx43 labeling. (A) A slice of SBF-SEM image demonstrates segmentation of ID (lavender bule) and gold labeled Cx43 beads (yellow). (B) 3D segmentation of reconstructed images illustrate closely packed strings of Cx43-gold particles (yellow) on the entire length of two parallel gap junction plaques at the ID (lavender blue). Bar = 5 μm.

Table 1

Hard Epon and Durcupan recipe.

Epon		**Durcupan**	
Component	**Volume (mL)**	**Component**	**Volume (mL)**
EMbed-812	5	A (epoxy)	5
DDSA	2.25	B (964 hardener)	5
NMA	3	C (964 accelerator)	0.15
BDMA	0.25–0.3	D (dibutyl phthalate)	0.05
Total	10.5		10.2

Table 2

Zeiss Gemini300 SEM with Gatan 3View image acquisition parameters.

keV	Working distance (nm)	FCC/chamber pressure (mBar)	Dwell time (μs/pixel)	XY resolution (nm)	Z resolution (nm)
1.2	7.4	40%/2.9E-03	2.0	3.5	50